




Analysis of the key signaling pathway of baicalin that induces autophagy in papillary thyroid cancer via an optical resonator

YI LAI,^{1,†} DAN RU,^{1,†} CHENHUAN DING,¹ CHEN WANG,¹ LING DING,¹ CENXIN LUO,¹ YUJIE QI,^{2,3} XIANFENG CHEN,^{2,3,4,6} HAILANG DAI,^{2,3,7}  AND HE LI^{1,5,8}

¹Department of Traditional Chinese Medicine, Department of Head and Neck Surgery, Renji Hospital, School of Medicine, Shanghai Jiao Tong University, No. 160 Pujian Road, Shanghai 200127, China

²School of Physics and Astronomy, Shanghai Jiao Tong University, No. 800 Dongchuan Road, Shanghai 200240, China

³State Key Laboratory of Advanced Optical Communication Systems and Networks, Shanghai Jiao Tong University, No. 800 Dongchuan Road, Shanghai 200240, China

⁴Collaborative Innovation Center of Light Manipulations and Applications, Shandong Normal University, Jinan 250358, China

⁵Shanghai Key Laboratory of Gynecologic Oncology, Shanghai Jiao Tong University, No. 160 Pujian Road, Shanghai 200127, China

⁶xfchen@sjtu.edu.cn

⁷hailangdai@sjtu.edu.cn

⁸lihe1972@hotmail.com

[†]These authors contributed equally to this work.

Abstract: Despite advances in cancer therapy, high mortality persists due to drug resistance and relapse. Developing selective anticancer agents with minimal toxicity and resistance remains crucial. Baicalin shows antitumor potential, but its mechanism against papillary thyroid carcinoma (PTC) remains unclear. We designed an optical resonator to monitor baicalin-membrane protein interactions, identifying NGFR as the key ATR-shifted target. Mechanistic studies revealed baicalin induces autophagy via the NGFR/MAPK/mTOR axis, validated through in vitro and in vivo models. These findings position baicalin as a promising PTC therapeutic with clinical translation potential.

© 2025 Optica Publishing Group under the terms of the [Optica Open Access Publishing Agreement](#)

1. Introduction

In recent decades, thyroid cancer is gaining more and more attention worldwide due to its high incidence rate. Further thyroid cancer ranks in 8th place for cancer incidence, and it is estimated more than 40,000 new cases in 2024 in USA [1–3]. Therein, based on difference in tumor origin and differentiation, thyroid cancer can be classified as papillary thyroid cancer (PTC), follicular thyroid cancer (FTC), medullary thyroid carcinoma (MTC) and anaplastic thyroid carcinoma. Among all subtypes, PTC accounts for more than 80–90% of cases, with a favourable prognosis [4,5]. However, it is reported about 2.4% patients developed invasive cancer, and advanced-stage disease and incidence-based mortality rates continue to increase [4]. PTC is mainly treated by surgery, supplemented with endocrine therapy, I131 therapy and molecular-targeted therapy. But, the standard treatment should be supervised due to the long treatment time, and more effective drugs should be explored. Therefore, identifying a natural drug for PTC is very important. Baicalin, a major bioactive flavone derived from *Scutellaria baicalensis*, has remarkable potentials in anti-bacterial, anti-inflammation, anti-tumor and immune modulating functions. Baicalin plays an antitumor role in a variety of tumors, which induced ferroptosis in osteosarcomas and gastric cancer, promoted antitumor immunity in hepatocellular carcinoma [6–11]. Moreover,

baicalin was reported to be related with autophagy in nasopharyngeal carcinoma, heart-injury and random-pattern skin flap [12–14].

Recently, autophagy is one of classic programmed cell deaths, and it degrades misfolded or useless proteins in the lysosomal lumen and recycled for another biosynthesis in conditions of hypoxia, starvation, stress and toxicity [15]. It is a highly conserved character from yeast to mammals, which helps to maintain homeostasis. Autophagy plays a bidirectional role in tumor progression, which plays either tumor-suppressing or tumor-promoting roles. AMPK/mTOR signal pathway is critical for autophagy, and the phosphorylates of AMPK could deactivate mTOR, which initiates autophagy [15]. However, the mechanism of baicalin in thyroid cancer and the relationship between baicalin and autophagy have not studied yet. Addressed this issue, a two-dimensional constrained optical resonator (TDCOR) is developed to carry out the relevant mechanism of action induces apoptosis diverse signaling pathways by baicalin. In this design, the use of double metal claddings which exhibit negative dielectric constant implies that the effective index of the guided modes and hollow core capillary can exist in the region of $0 < N < 1$, which is usually prohibited for the conventional guided modes and the surface plasmon resonance [16–18]. Excitation of the ultrahigh order modes (UOMs) with $N \rightarrow 0$ [17], which means group velocity approaches zero maximizes the interaction between membrane proteins and baicalin. Thus it is possible to enhance the sensitivity of the platform. Experiment results have proved that the TDCOR provide an effective way to monitor drug interactions in real time using membrane proteins (NGFR, AMPK, CDH3, HSPA8 and MAGI2 which are screened by RNA-sequencing after the baicalin has been used to inhibit PTC cell) of cancer cells process via ATR shifts. Thus we designed the following study to explore the function of baicalin in papillary thyroid cancer. According to the results of TDCOR, baicalin induce autophagy via NGFR/MAPK/mTOR pathway in papillary thyroid cancer. Furthermore, we design a series of in vitro and in vivo experiments to proof the key signaling pathway which has screened. Therefore, it could establish baicalin as an effective and safe compound for papillary thyroid cancer treatment as well as help to translate its potential from bench to bedside.

2. Results and discussions

2.1. Baicalin inhibits the proliferation, migration, and invasion of PTC cells

The 24 and 48 h cell viabilities of bc pap cells were measured by CCK8 assay. Baicalin could inhibit the proliferation of bc pap cells in a dose- and time-dependent manner. The IC₅₀ values of 24 and 48 h were 158.8 and 113 μ M, respectively (Fig. 1(b)). In addition, baicalin inhibited the colony formation of thyroid cancer cells by the increasing of concentration (Fig. 1(c)). Wound healing assay showed baicalin inhibited migration of bc pap cells, and the migrated areas of three different concentrations were 93.63 ± 1.16 , 84.16 ± 3.00 and 60.55 ± 3.86 . Moreover, the transwell assay showed the punctuated cells of migration assay of 0, 80 and 160 μ M were 254.0 ± 8.89 , 91.67 ± 14.22 , 22.33 ± 4.73 , and 90.33 ± 9.07 , 41.67 ± 3.51 , 13.67 ± 1.53 of invasion assay, respectively (Fig. 1(d)). The 24 h apoptosis rates of thyroid cell lines of 0, 80 and 160 μ M were $1.86 \pm 0.30\%$, $31.93 \pm 4.66\%$, and $53.87 \pm 12.31\%$ (Fig. 1(e)).

2.2. Baicalin induces autophagy and apoptosis in thyroid cancer cells

From RNA sequencing, we compared untreated and baicalin treated thyroid cells, and found 3226 differential genes, including 1938 upregulating genes and 1288 downregulating genes (Fig. 2(a) and Supplement 1 Appendix, Fig. S1). Furthermore, we completed GO and KEGG enrichment analysis, and found baicalin might related to postsynaptic specialization membrane (Fig. 2(b)-(c) and Supplement 1 Appendix, Fig. S1).

According to the results of GO and KEGG enrichment analysis [Fig. 2(a-e2)], we rough found baicalin might related to postsynaptic specialization membrane, and the expression of NGFR,

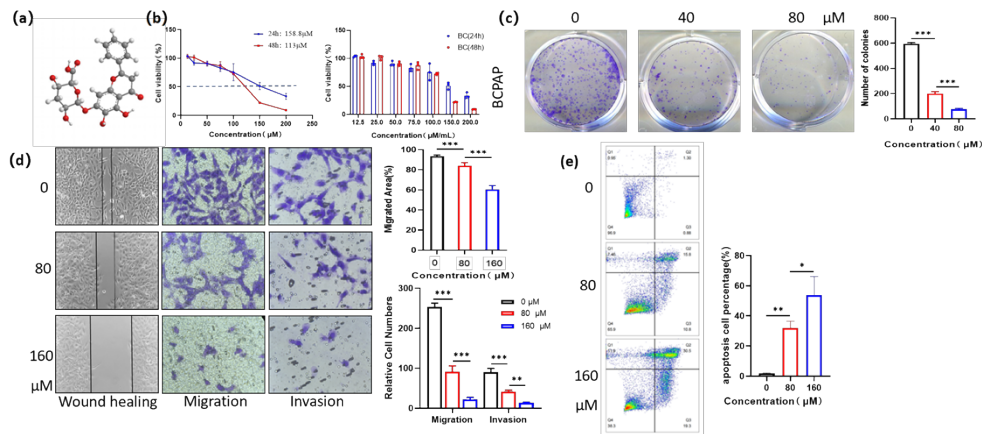


Fig. 1. (a) The molecule structure of baicalin. (b) The 24 h and 48 h cell viabilities of bcpap cells by CCK8 assay (c) The colony formation assay of bcpap cells after 10 days under baicalin treatment (d) The 24 h wound healing assay and 48 h migration and invasion transwell assay of bcpap cells under baicalin of 0, 80, 160μM($\times 20$) (e) The 24 h apoptosis rates of bcpap cells under baicalin of 0, 80, 160μM with flow cytometry. The results were represented the means \pm SD of triplicate independent experiments. *** $P < 0.001$, ** $P < 0.01$, * $P < 0.05$.

AMPK, CDH3, HSPA8 and MAGI2 which were connected to this pathway were upregulated, respectively. Figure 2 (h) and SVIII Appendix, Fig. S10(a) shows the NGFR, AMPK, CDH3, HSPA8 and MAGI2 structures. Therefore, we used TDCOR to analysis and screen molecule which has interaction with baicalin. As shown in Fig. 2 (k), baicalin and NGFR, AMPK, CDH3, HSPA8 and MAGI2 has been injected into resonator, and computer-controlled $\theta/2\theta$ goniometer performs angular scans while the intensity of the reflected beam is detected by a photodiode from 20 to 120 mins, respectively. We can find that the ATR dip has stood at especial θ degree apart between each other in different time besides beginning and ending time when NGFR has been injected into TDCOR. The observed ATR dip shift and refractive index (RI) alterations originates from NGFR-baicalin binding. Whilst the ATR dip of AMPK has stand at θ degree apart between each other. And the series of ATR dips of CDH3, HSPA8 and MAGI2 coupling angle difference is not especially noticeable. Compared with NGFR, CDH3, HSPA8 and MAGI2 ATR dip coupling angle, we can obtain that NGFR molecular structure has significant changed by injecting baicalin, and the θ shift 0.20 degree from 0 to 120 mins. And the θ shift 0.15 degree for CDH3, HSPA8 and MAGI2, respectively. As the θ shift display (Fig. 2 (k)), we can conclude that NGFR molecule structure can easily to be changed by interaction with baicalin. According to the results of analysis and screening by ATR shift from TDCOR, the NGFR is the target of baicalin action point to induce autophagy. Therefore, we design a series of experiments to proof the key signaling pathway which has screened in following part.

From detection results of TDCOR, we inferred baicalin suppressed thyroid cancer by AMPK/mTOR pathway in autophagy related manner. Next, we analyzed correlation between NGFR and autophagy related gene by TIMER2.0 [19,20] based on TCGA database, and found CASP3, CASP9, ATG9A and MAP1LC3B positively relative with NGFR (Fig. 3(b)). To explore the relationship between baicalin and NGFR, docking analysis was performed and the binding energy between NGFR and baicalin was -8.322 kcal/mol, while the binding energy between AMPK and baicalin was -9.433 kcal/mol. We indicated baicalin bind to protein NGFR and AMPK directly.(Fig. 3(c)) In addition, the scores showed autophagy was induced in papillary thyroid cancer, and expression of NGFR was elevated in autophagy process. Moreover, COIP

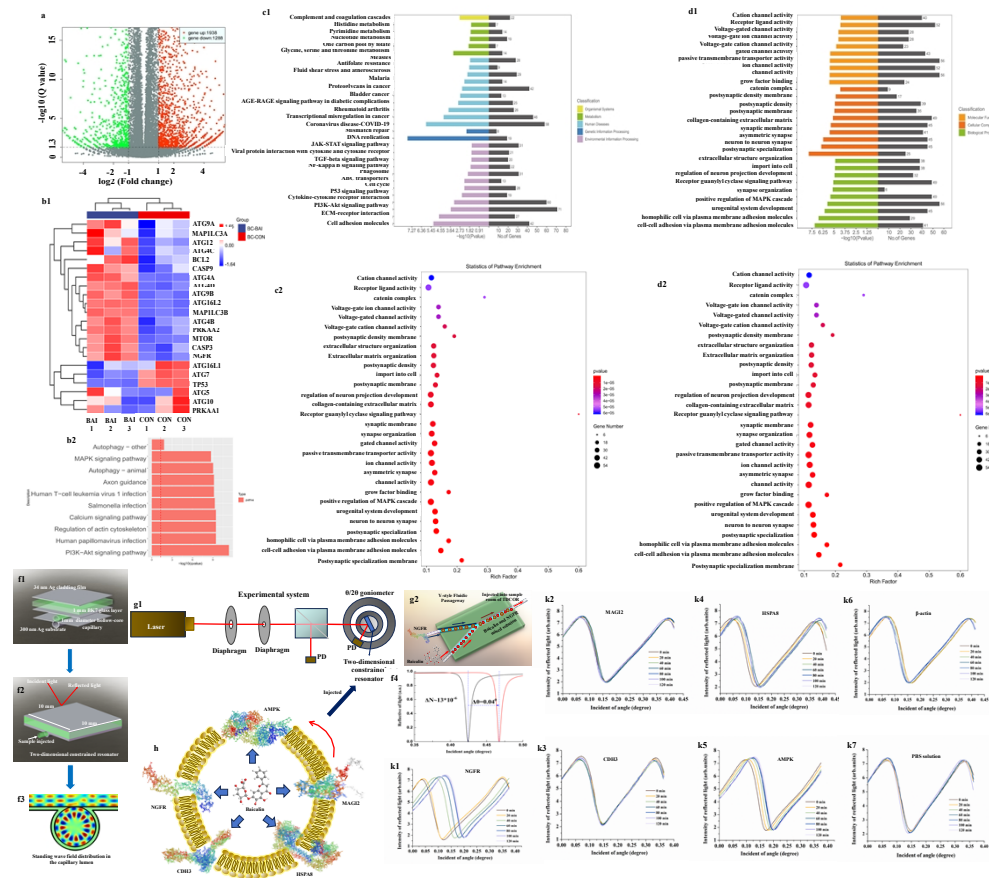


Fig. 2. RNA seq and experimental system and optofluidic resonator. (a-c) The differential genes between baicalin treated and control PTC cells (d1, d2) The GO enrichment analysis between baicalin treated and control PTC cells (e1,e2) The KEGG enrichment analysis between baicalin treated and control PTC cells. (f1) and (f2) the structure of two-dimensional constrained optical resonator (TDCOR); (f3) The effective index of the guided modes and hollow core capillary can exist in the region of $0 < N < 1$, which is usually prohibited for the conventional guided modes and the surface plasmon resonance. (f4) reflectivity of light R and coupled angle θ changed, when the refractive index of the sample changed. The refractive index of the sample changed and the ATR position shifted, such that the ATR dip would shift. (g1-g2) Experimental setup; (k1-k7) NGFR, AMPK, CDH3, HSPA8, MAGI2 structures (<https://swissmodel.expasy.org/>), β -actin and PBS solution and the ATR dip would shift when baicalin interaction.

assays were performed to verify interaction between protein AMPK and NGFR, and results showed NGFR was related to AMPK/mTOR pathway in thyroid cancer (Fig. 3(d)).

After 24 hours of baicalin treatment, autophagosomes were observed by transmission electron microscope (TEM) and fluorescence microscope in thyroid cancer cells. TEM showed autophagosomes were induced under baicalin treatment (Fig. 3(e)). Moreover, bcpap cells were infected with stubRFP-sensGFP-LC3 lentivirus, and yellow-green fluorescence spots (autophagosomes) were observed by merging the red and green fluorescence signals under fluorescence microscope. After baicalin treatment, yellow-green fluorescence spots were increased, which indicated autophagy was induced under baicalin treatment (Fig. 3(f)).

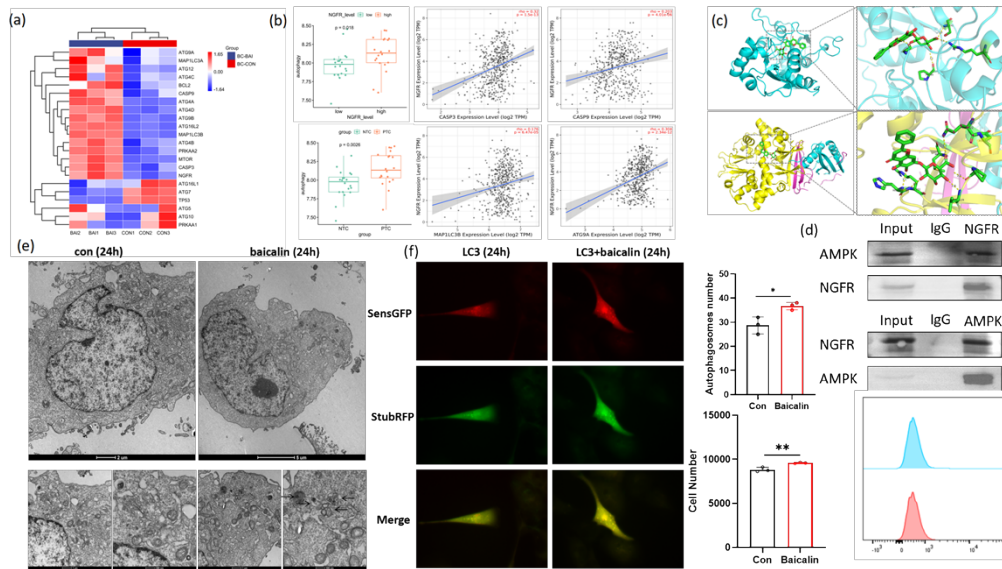


Fig. 3. (a) Heatmap of autophagy and apoptosis markers between baicalin treated and control PTC cells. (b) The scores of autophagy, NGFR and thyroid cancer. (c) The molecular structure of NGFR and AMPK, and binding energy between baicalin by AutodockVina 1.2.2, the interaction value was -8.322 kcal/mol and -9.433 kcal/mol. (d) The COIP of AMPK and NGFR in bcpap cells. (e) The autophagosomes images by transmission electron microscope in baicalin treated and untreated PTC cells (Arrows indicated autophagosome). (f) The autophagosomes photoed by fluorescence microscope in baicalin treated PTC cells ($\times 40$) and autophagy flux with flow cytometry. $**P < 0.01$.

2.3. Baicalin promotes autophagy and apoptosis by NGFR/AMPK/mTOR signaling pathway in thyroid cancer cells

The 24 and 48 h cell viabilities of bcpap and bc-shNGFR cells were measured by CCK8 assay. Baicalin could inhibit the proliferation of both cells in a dose- and time-dependent manner, and the inhibitory effects of bcpap was better than bc-shNGFR. Furthermore, the 24 h IC₅₀ values of two cells were 158.8 μ M and 199.3 μ M, and the 48 h IC₅₀ values of two cells were 113 μ M and 151.6 μ M, respectively (Fig. 4(a)). The colonies of bcpap cells under 0, 80 μ M baicalin and AMPK, mTOR inhibitor were 711.67 \pm 12.66, 206.00 \pm 7.211, 274.33 \pm 7.10 and 83.00 \pm 5.00, and 700.33 \pm 11.59, 529.00 \pm 18.74, 610.667 \pm 10.693, and 489.67 \pm 15.01 of bc-shNGFR cells, respectively (Fig. 4(b)). The 24 h apoptosis rates of bcpap cells of 0, 160 μ M and AMPK, mTOR inhibitor were 1.92 \pm 0.18%, 48.67 \pm 4.12%, 9.81 \pm 0.84%, 71.15 \pm 3.10%, 2.65 \pm 0.41%, 25.46 \pm 0.99%, 5.69 \pm 0.38%, 34.92 \pm 5.03% for bc-shNGFR cells (Fig. 4(c)). Wound healing assay showed the migrated areas of bcpap cells under 0, 160 μ M and AMPK, mTOR inhibitor were 89.62 \pm 1.84, 60.25 \pm 4.16, 85.47 \pm 4.39, 41.76 \pm 1.49 and 90.21 \pm 1.64, 80.07 \pm 1.42, 73.96 \pm 3.94, 67.57 \pm 2.10 for bc-shNGFR cells. Moreover, the transwell assay showed the punctuated bcpap cells of migration assay of 0, 160 μ M and AMPK, mTOR inhibitor were 484.33 \pm 20.13, 37.67 \pm 3.512, 165.00 \pm 6.65, 47.33 \pm 3.512, and 90.33 \pm 9.07, 19.00 \pm 2.00, 50.67 \pm 1.53, 10.67 \pm 1.53 of invasion assay, and punctuated bc-shNGFR cells of migration assay of 0, 160 μ M and AMPK, mTOR inhibitor were 492.33 \pm 16.62, 198.67 \pm 8.62, 254.00 \pm 8.89, 96.67 \pm 5.51 and 93.33 \pm 6.81, 42.33 \pm 3.512, 76.00 \pm 2.65, 28.00 \pm 3.606 of invasion assay respectively (Fig. 4(e)). From above, baicalin inhibited proliferation, migration, invasion and promoted apoptosis of bcpap cells, and knocking down NGFR could reverse.

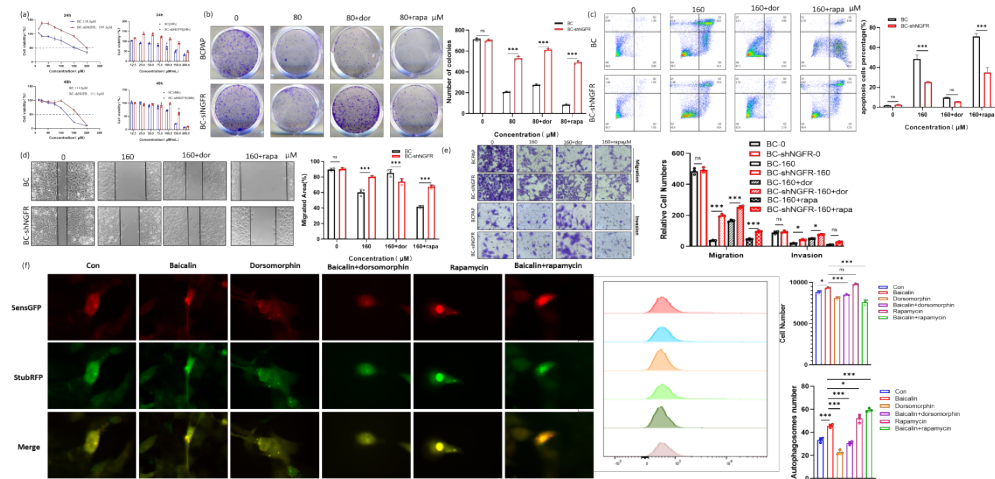


Fig. 4. (a) The 24 h and 48 h cell viabilities of bc-pap and bc-shNGFR cells by CCK8 assay (b) The colony formation assay of bc-pap and bc-shNGFR cells after 10 days under baicalin treatment (c) The 24 h apoptosis rates of bc-pap cells under baicalin of 0, 160 μ M combined with dorsomorphin or rapamycin with flow cytometry. (d) The 24 h wound healing assay of bc-pap cells and bc-shNGFR under baicalin of 0, 160 μ M combined with dorsomorphin or rapamycin. (e) 48 h migration and invasion transwell assay of bc-pap cells and bc-shNGFR under baicalin of 0, 160 μ M combined with dorsomorphin or rapamycin ($\times 20$). (f) The autophagosomes photoed by fluorescence microscope in baicalin/dorsomorphin/rapamycin treated PTC cells ($\times 40$). and autophagy flux with flow cytometry. The results were represented the means \pm SD of triplicate independent experiments. *** $P < 0.001$, ** $P < 0.01$, * $P < 0.05$, ns had no significance.

After baicalin treatment, yellow-green fluorescence spots increased, which indicated autophagy was initiated. Meanwhile, yellow-green fluorescence spots faded after 24 h treatment of dorsomorphin (AMPK inhibitor), while green fluorescence signals quenched and merged signals showed orange meaning autolysosome appeared after rapamycin (mTOR inhibitor) treatment (Fig. 4(f)).

2.4. Baicalin suppress tumor growth of tumor bearing mice by NGFR/AMPK/mTOR signaling pathway

Combined with results above, we speculated that baicalin may inhibit thyroid cancer through the NGFR/AMPK/mTOR pathway. We designed an in vivo experiment of six groups to verify this hypothesis. Bc-pap or bc-shNGFR cell suspension was transplanted subcutaneously in balb/c-nu mice and randomly divided into six groups: BC-con group, BC-low group, BC-high group, BC-shNGFR-con group, BC-shNGFR-low group, and BC-shNGFR-high group. Low and high dose group mice undertook intraperitoneal injection of baicalin 40 mg/kg and 80 mg/kg everyday, while control group undertook PBS solutions. After 28 days of invention, we executed mice and removed the subcutaneous tumors for immunofluorescence detection. It was found that the tumor of the low and high group was significantly smaller than the control group, $P < 0.001$, and showed no significance between shNGFR-low and shNGFR-high group. It inferred that the baicalin can effectively inhibit the growth of thyroid cancer tumors (Fig. 5(a-c)).

As shown in Fig. 5(d), the caspase3 expression was elevated by concentrations of baicalin, and the intensity in BC-high group was significantly higher than that in BC-shNGFR-high group, $P < 0.05$; There was no significant difference between BC group and BC-shNGFR

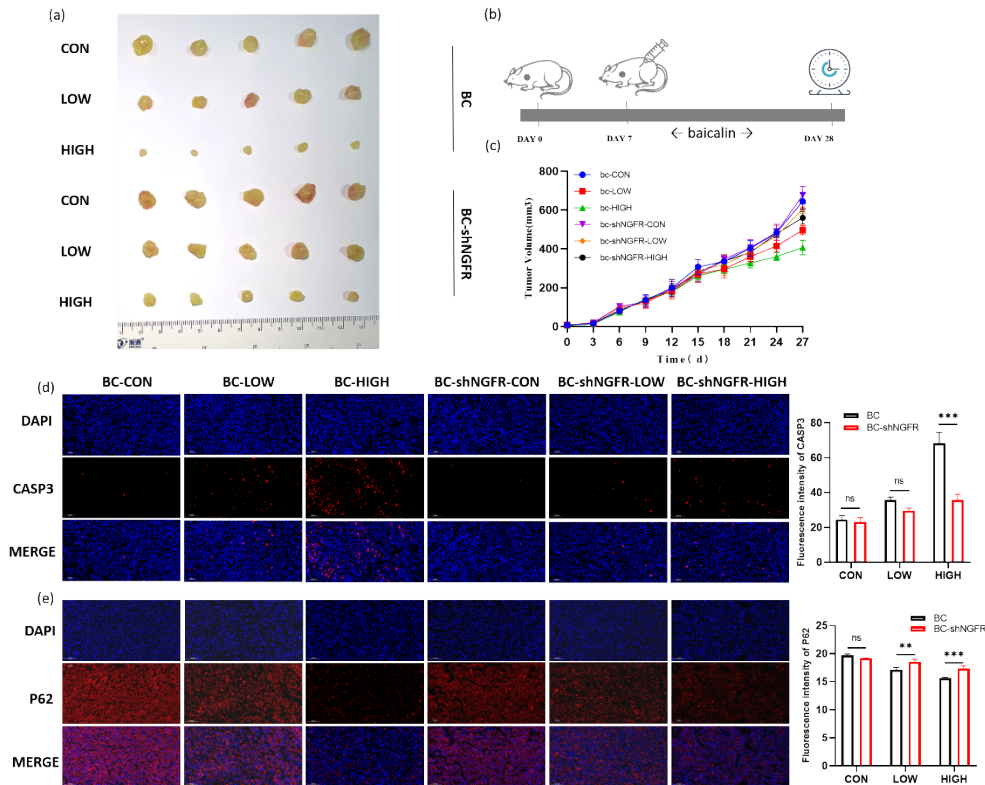


Fig. 5. Tumor growth in balb/c-nu mice treated with different concentrations of baicalin, and immunofluorescence detection of caspase3 and p62 in tumor. (a) Subcutaneous tumor growth in balb/c-nu mice treated with baicalin. (b) The illustration of balb/c-nu mice model (c) Tumor growth curves of tumor bearing mice. (d-e) The intensity of caspase3 and p62 in tumor tissues were detected by immunofluorescence under different drug concentrations (magnification $\times 400$), and quantitative statistics of d-e. ** $P < 0.01$, *** $P < 0.001$, and ns had no statistical difference.

group of con and low groups ($P > 0.05$). From Fig. 5(e), the p62 expression was decreased by concentrations of baicalin, and the intensity in BC-high group was significantly lower than that in BC-shNGFR-high group, $P < 0.05$; the intensity in BC-low group was significantly lower than that in BC-shNGFR-low group, $P < 0.05$; There was no significant difference between BC-con group and BC-shNGFR-con group ($P > 0.05$). Above results indicated that baicalin could increase the expression of caspase3 and weaken the expression of p62 in thyroid cancer by targeting NGFR, which concluded baicalin could induce autophagy and apoptosis by the NGFR/AMPK/mTOR pathway.

2.5. Side effects of baicalin in thyroid cancer tumor-bearing mice

We sacrificed mice and removed main organs such as heart, liver, spleen, lung and kidney to perform HE staining, and found no significant difference in morphology among all groups (Fig. 6(a)). Meanwhile, there was no significant difference between groups in liver and kidney biochemical indexes, such as ALT, AST, ALP, BUN, CRE (Fig. 6(b)). We conducted cck8 assays in liver, kidney, thyroid and myocardial normal cell lines for drug cytotoxicity test (AML12, mice liver cell line; HK2, human kidney cell line; NTHY-ori 3-1, human thyroid cell line; H9c2, Rat

myocardial cell line). As a result, the normal cell viabilities were maintained as high as 80% after incubating at the concentration of 240 μM for 24 hrs (Fig. 6(c)). We concluded baicalin had no significant side effects of main organs within the effective therapeutic dose range in thyroid cancer.

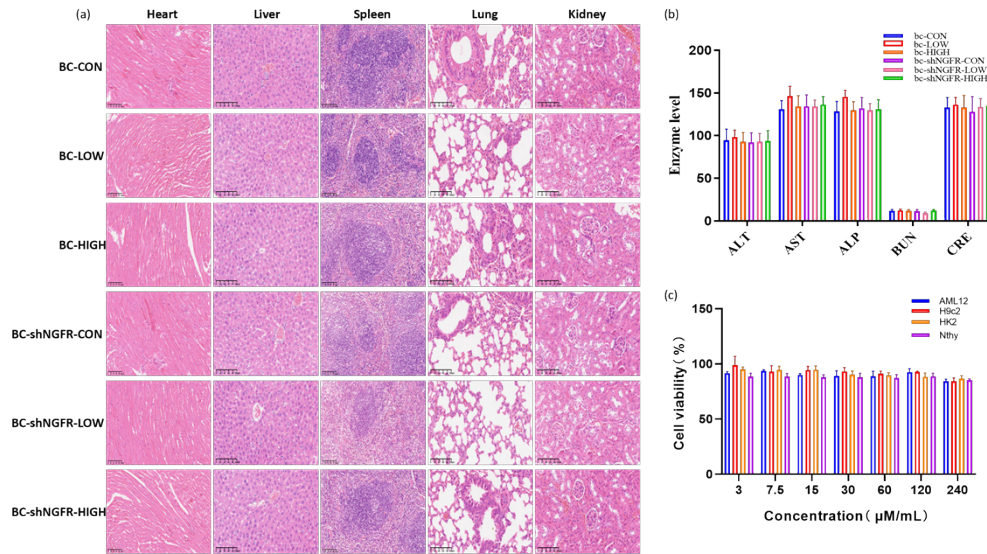


Fig. 6. Safety evaluation of balb/c-nu mice in different groups. (a) Representing H&E staining images of major organs (heart, liver, spleen, lung and kidney) treated with different concentration of baicalin after 21 days (scale bar: 50 μm , magnification $\times 200$). (b) Liver and kidney biochemical indexes treated with baicalin after 21 days. (c) Normal cell viabilities of different baicalin concentrations at 24 h.

2.6. Discussions

The revealing rate of thyroid cancer is raising these years mainly due to ultrasound technology [3]. However, more and more patients were diagnosed advanced stage, which leads to poor prognosis. Thanks to immune therapy, median progression-free survival of advanced patients can reach 18.3-20.1 months, especially for radioiodine-refractory thyroid cancer [2]. However, adverse effects like hand-foot skin reaction, hypertension, diarrhoea always annoy patients, and more effective and mild drug is needed. Traditional Chinese medicines (TCM) have been used for thousands of years which provide an alternative treatment for cancer. As one of the most traditional medicinal plants, *Scutellaria baicalensis* has been used to treat fever, cough, diarrhea and infection for more than 2000 years. Baicalin is a flavonoid isolated from the dried root of *Scutellaria baicalensis*, and it has a wide range of pharmacological effects. Moreover, baicalin plays an antitumor role in a variety of tumors, which induced ferroptosis through Hrf2/xCT/ GPX4 axis in osteosarcomas [9], enhanced the efficacy of 5-Fluorouracil in gastric cancer by promoting ROS-mediated ferroptosis [8,11], and regulated the radioresistance of CNE-2R cells via autophagy in nasopharyngeal carcinoma [6]. Until now, the drug target identification and validation is still a time-consuming and laborious work, while technique including phenotypic screening, biochemical screening and affinity-based screening have the disadvantages in complicated sample processing and time-consuming. Our study aimed to explore an effective and efficient method to predict drug target by means of optical resonator. We designed a two-dimensional constrained optical resonator (TDCOR) to detect ATR dip shift.

This means has an advantage of a high sensitivity of 700°/RIU for the TE and TM modes, and NGFR was selected from four candidates.

Nerve Growth Factor Receptor (NGFR), also named P75 NTR, is known as one of neurotrophin receptors and pro-neurotrophins receptors, which participate in neurotrophin development [21,22]. It belongs to the TNF-receptor gene family. In particular, recent researches showed NGFR enrolled in tumor growth and dissemination [23,24]. NGFR always played as tumor suppressor and participated in blocking cell cycle progression and inducing apoptosis in gastric, bladder, and prostate cancers [25,26]. However, the mechanism of NGFR in thyroid cancer is not clear [27,28]. Our study showed baicalin related to autophagy in papillary thyroid cancer via NGFR/AMPK/mTOR pathway, which interacts with tumor progression.

Autophagy is a fundamental and ubiquitous biological event conserved in mammals including humans. Basically, autophagy is a catabolic process that cellular components including small molecules and damaged organelles are degraded for recycle to meet the energy needs, especially under the extreme conditions, such as hypoxia, stress, starvation, toxicity. Autophagy classically contains three formats, namely, macroautophagy, microautophagy and chaperone-mediated autophagy. The macroautophagy is the most common one and is regarded as autophagy [15]. Autophagy is widely involved in tumor biological behaviors including cancer stem cell (CSC) survival, cell death, distant metastasis, drug resistance and so on. The dysregulated autophagy has indicated to be involved in thyroid cancer progression [15]. It is reported autophagy closely related with thyroid function and prognosis of thyroid cancer, it could downregulate sodium/iodide symporter (NIS)-mediated iodide uptake via ROS/AMPK/mTOR pathway [29]. Studies showed autophagy was associated with differentiation of thyroid cancer, especially in braf/ras-mutant cancer, which indicated the resistance of RAI therapy [15]. It was reported inhibition of mTOR suppressed autophagy, thus reduced EMT and metastasis of bc pap cell lines [30]. Furthermore, as another way of cell death, apoptosis is closely linked to autophagy in a variety of cancers. Electroscope is used for confirmation and identification of autophagy, and all stages of autophagy can be detected by it. In addition, LC3 and p62 are markers of autophagy, the increased ratio of LC3I/LC3II and decreased p62 protein indicate the initiation of autophagy. Our results showed increased signals under TEM and elevation of LC3I/LC3II ratio and decline of p62 in tumor bearing mice after baicalin intervention. Results indicated baicalin induced autophagy through NGFR/AMPK/mTOR pathway in thyroid cancer. AMPK/mTOR pathway works as upstream of autophagy, and deactivation of mTOR initiated autophagy under condition of deprivation of nutrients.

3. Conclusion

We provide an effective way to monitor drug interactions in real time using membrane proteins (NGFR, AMPK, CDH3, HSPA8 and MAGI2 which are screened by RNA-sequencing after the baicalin has been used to inhibit PTC cell) of cancer cells process via ATR shifts. According to the results of TDCOR, baicalin induce autophagy via NGFR/AMPK/mTOR pathway in papillary thyroid cancer. Further, it unveils exciting opportunities in clear and rapid analysis of the molecular antibacterial, anti-inflammation, anti-tumor and immune modulating functions mechanism of herbs in Chinese medicine.

4. Materials and methods

4.1. Chemicals

Dulbecco's modified Eagle's medium (DMEM) and fetal bovine serum (FBS) were obtained from Invitrogen (Gibco, USA). Dimethylsulfoxide (DMSO) and Cell Counting Kit-8 (CCK8) were obtained from TargetMOI (Boston, MA). Lentivirus sh-RNA NGFR and stubRFP-sensGFP-LC3 lentivirus was purchased by Genechem (Shanghai, China). Baicalin was purchased from LC

Laboratories (LC Laboratories, Woburn, MA). Rapamycin (RAPA) was obtained from Cell Signaling Technology (CST, USA). Total AMPK, total mTOR and phosphorylated mTOR antibodies were obtained from Cell Signaling Technology (CST, USA). The NGFR antibody was obtained from Abcam (USA), and β -actin and HRP-conjugated secondary antibody from Abcam (USA).

4.2. Cell lines and cell cultures

Human papillary thyroid cancer cell lines bcpap were purchased from National collection of authenticated cell cultures (Shanghai, China). Bcpap cell lines were cultured in DMEM supplemented with 10% FBS and 1% penicillin-streptomycin antibiotic mixture (Gibco, USA) at 37 °C in an atmosphere of 5% CO₂. Furthermore, AML12, HK2, NTHY-ori 3-1, H9c2 were purchased from National collection of authenticated cell cultures (Shanghai, China) for drug toxicity detection. AML12 was cultured in DMEM/F-12(1:1) medium supplemented with 10% fetal bovine serum (FBS), 1% Insulin-transferrin-sodium (ITS) and 40 ng/ml Dexamethasone, other cell lines were cultured in DMEM supplemented with 10% fetal bovine serum and penicillin-streptomycin antibiotic mixture (Gibco) at 37 °C in an atmosphere of 5% CO₂.

4.3. RNA sequencing

RNA of baicalin-treated and untreated cells was extracted. Differences in gene expression profiles between the two groups were represented by volcano maps, with vertical dashed lines representing up-regulated and down-regulated differences of 2.0 times (log₂ conversion), respectively, and up-regulated genes represented by red dots in the figure. The volcano map of differentially expressed genes was drawn using the R language ggplots2 software package, and the results showed that there were differences in the gene expression profiles of mice after dual drugs treatment.

In order to further analyze the function of differentially expressed genes after baicalin administrations, we used topGO to conduct the related analysis of GO enrichment, and KEGG pathway to annotate the differential genes and the gene list and number of each pathway, and hypergeometric distribution method was used to obtain P values ($P < 0.05$). Use genescloud platform (<https://www.genescloud.cn>) for data analysis, and pheatmap package (V1.0.8) developed by heat map tool drawing heat maps.

4.4. Autodock

To analyze the binding affinities and modes of interaction between the drug candidate and their targets, AutodockVina 1.2.2, a silico protein–ligand docking software was employed. The molecular structures of NGFR and AMPK were retrieved from PubChem Compound (<https://pubchem.ncbi.nlm.nih.gov/>). The 3D coordinates of NGFR (PDB ID: 4F42; resolution: X-RAY DIFFRACTION 2.38 Å), AMPK (PDB ID: 4EAG; resolution: were: X-RAY DIFFRACTION 2.701 Å) downloaded from the PDB (<http://www.rcsb.org/pdb/home/home.do>). For docking analysis, all protein and molecular files were converted into PDBQT format with all water molecules excluded and polar hydrogen atoms were added. The grid box was centered to cover the domain of each protein and to accommodate free molecular movement. The grid box was set to 30 Å × 30 Å × 30 Å, and grid point distance was 0.05 nm. Molecular docking studies were performed by Autodock Vina 1.2.2 (<http://autodock.scripps.edu/>).

4.5. CCK8 assay

Cell viability was detected via Cell Counting Kit-8 (CCK-8) assay. bcpap cell lines were incubated with baicalin for 24 to 48 h, and then replaced with 100uL 10% CCK-8 reagent (TargetMOI, China) for 1 h at 37C. The OD of each well was measured at 450 nm using a Thermo Scientific Varioskan Flash (Thermo Fisher Scientific, USA).

4.6. Colony formation

Bcpap cells were seeded at a concentration of 100 cells/well into 12-well plates in DMEM supplement. After 24 h of culture, baicalin of different concentration were added into plates, and change solutions every 3 days. Cells were fixed with 4% formaldehyde for 15 mins, stained with 0.5% crystal violet for 15 mins and plates were observed by scanner after 10 days.

4.7. Cell invasion and migration

Cell invasion and migration was measured using 24-well transwell chamber (Corning Costar) precoated with or without Matrigel. Cells in serum-free medium were seeded at 1×10^5 per well in the top chamber, while 20% FBS medium with different concentration drugs was added in the bottom chamber. After incubation for 24 h at 37 °C, cells were fixed with 4% formaldehyde for 15 mins, stained with 0.5% crystal violet for 15 mins and counted.

4.8. Wound healing

Bcpap cells were seeded at a concentration of 1×10^5 cells/well into 12-well plates in DMEM supplement. Cells were incubated overnight yielding confluent monolayer for wounding. Wound tracks in the monolayer were scored in each well using a 200 μ L pipette tip. Then the suspended cells were washed twice with PBS, and the wounded cell monolayer was incubated in 5%FBS medium with different concentration of baicalin for 24 h. Photographs of the wound area were captured at the 0 and 24 h with microscope (Olympus America Inc, USA).

4.9. Cell lentiviral transfection

Bcpap cells were plated at a density of 1×10^5 cells per 60-mm dish for 24 h and then infected with the stubRFP-sensGFP-LC3 or shNGFR lentivirus in DMEM. Forty-eight hours after infection, the cells were re-plated and selected with puromycin for 48 hours. The resulting NGFR-knockdown and stubRFP-sensGFP-LC3 bcpap cells were expanded for further analysis. The transfection effects were confirmed by RT-PCR.

4.10. Animals and in vivo model

All animal experiments were performed in accordance with the national and institutional guidelines for animal care and were approved by the Animal Experiment Ethics Committee of Shanghai Renji hospital affiliated to Shanghai Jiaotong University School of Medicine. Mice were maintained under specific pathogen free conditions and randomly assigned to each experimental group. All mice were supplied with sterile drinking water and fed freely. Six to eight weeks old BALB/c-nu mice were used for the studies. BALB/c-nu mice were injected with 5×10^6 bcpap cells. All cells were injected subcutaneously into the flank. All control groups was fed with PBS 50 ml/kg/d, and baicalin (Macklin, Shanghai) were diluted into 10 mM solution using DMSO solution, drugs were further diluted on the day of experiment.

4.11. Flow cytometry

We seeded bcpap cells (1×10^6 cells) in every T25 culture flask, and we added different concentrations of baicalin after 24 h incubation. After another 24 h, we collected and washed the supernatant and the adherent cells and added 1 μ L of annexin and propidium iodide to test solutions respectively.

FITC signal(GFP) was detected in stubRFP-sensGFP-LC3 bcpap cells, which was illustrated as autophagy flux. The samples were detected by LSR Fortessa X-20 or Celesta Flow cytometry system, and analyzed by Flow Jo software.

4.12. Immunofluorescence

The mice tissues were fixed with formaldehyde and embedded in paraffin. Subsequently, the tissue samples were cut into 4 μm thickness, deparaffinized in xylene, and rehydrated through graded ethanol solutions to analyze caspase3, P62 expression. The sections were deparaffinized and rehydrated, then blocked with 3% bovine serum albumin (BSA) for 30 min. The sections were next incubated with anti-CASP3, anti-P62 antibody (Proteintech, China) overnight at 4 °C and Cy3-labeled secondary antibody for 1 h at 37 °C, followed by nuclear staining with DAPI for 10 mins at room temperature. The staining results were observed by Nikon confocal laser microscope (Eclipse Ti-SR, Nikon) and imaging system (DS-U3, Nikon). The fluorescence intensity quantification were analyzed with the Image J software.

4.13. TEM (Transmission electron microscope)

Cells were collected and fixed in 2.5% glutaraldehyde overnight. Then the cells were treated with 1% osmic acid 0.1 M phosphate buffer PBS (PH7.4) was fixed at room temperature (20°C) for 2 h. The tissue was progressively dehydrated with 50%-70%-80%-90%-95%-100%-100% alcohol. After a second rinsing, cells were dehydrated with graded acetone and finally embedded in Quetol 812. Ultrathin sections were observed under an electron microscope (FEI, USA).

4.14. Western blotting

Cells were lysed in RIPA buffer containing protease inhibitors, and protein concentrations were determined using a BCA assay. Samples were denatured by boiling in loading buffer (5 min, 100°C), and then equal amounts of protein (20-50 μg) were separated by SDS-PAGE (12% gel) at 110 V for 1.5 hr. Next, proteins were transferred onto PVDF membranes using a wet transfer system (200 mA, 1.5 hr, 4°C), and blocked with blocking buffer for 1 hr at room temperature. Primary antibodies such as anti- β -actin (A01015, 1:5000 Abbkine); anti-NGFR (8238), anti-mTOR (2972, 1:1000, CST); anti-Becn1 (11306-1-AP), anti-ATG5 (10181-2-AP, 1:1000, Proteintech) were diluted and incubated overnight at 4°C. Membranes were washed 3 times with TBST, then incubated with HRP-conjugated secondary antibodies (1:5000) for 1 hr at RT. β -actin served as a loading control. Results were visualized using ECL substrate and quantified by ImageJ software.

4.15. Statistical analysis

Statistical analyses were conducted using Graphpad Prism 8 software. Results are expressed as mean \pm standard error of the mean (S.E.M.). The significance of differences among experimental groups was determined by ANOVA analysis. The differences are considered statistically significant at $P < 0.05$.

Funding. Medical and Industrial Cross Project of Shanghai Jiaotong University (YG2023QNB08); Shanghai Municipal Health Commission industry clinical research project (20234Y0089); National Natural Science Foundation of China (12104298, 82374163, 82174135, 12192252); Science and Technology Commission of Shanghai Municipality Major Project (2019SHZDZX01-06); Natural Science Foundation of Shanghai Municipality (23ZR1428400); Shanghai Health Commission Traditional Chinese Medicine (2022QN068).

Acknowledgments. The authors acknowledge support from the state Key Laboratory on Fiber Optic Local Area Communication Networks and State Key Laboratory of Metal Matrix Composites, and they also thank the Ruijin Hospital.

Disclosures. The authors declare no conflicts of interest.

Data Availability. Data underlying the results presented in this paper are not publicly available at this time but may be obtained from the authors upon reasonable request.

Supplemental document. See [Supplement 1](#) for supporting content.

References

1. J Ferlay, M. Colombet, I Soerjomataram, *et al.*, "Estimating the global cancer incidence and mortality in 2018: GLOBOCAN sources and methods," *Int. J. Cancer* **144**(8), 1941–1953 (2019).

2. DW Chen and Brian H H Lang, "Thyroid cancer," *Lancet* **401**(10387), 1531–1544 (2023).
3. R. L. Siegel, A. N. Giaquinto, A. Jemal, *et al.*, "Cancer statistics, 2024," *Ca-Cancer J. Clin.* **74**(1), 12–49 (2024).
4. U. C. Megwalu and P. K. Moon, "Thyroid Cancer Incidence and Mortality Trends in the United States: 2000-2018," *Thyroid* **32**(5), 560–570 (2022).
5. M Pizzato, M. Li, J Vignat, *et al.*, "The epidemiological landscape of thyroid cancer worldwide: GLOBOCAN estimates for incidence and mortality rates in 2020," *Lancet Diabetes Endocrinol.* **10**(4), 264–272 (2022).
6. M Ke, Z. Zhang, B. Xu, *et al.*, "Baicalein and baicalin promote antitumor immunity by suppressing PD-L1 expression in hepatocellular carcinoma cells," *Int. Immunopharmacol.* **75**, 105824 (2019).
7. YJ Fu, B. Xu, S. W. Huang, *et al.*, "Baicalin prevents LPS-induced activation of TLR4/NF-kappaB p65 pathway and inflammation in mice via inhibiting the expression of CD14," *Acta Pharmacol Sin* **42**(1), 88–96 (2021).
8. S Singh and Abha Meena, "Baicalin mediated regulation of key signaling pathways in cancer," *Pharmacol. Res.* **164**, 105387 (2021).
9. RJ Wen, X. Dong, H. W. Zhuang, *et al.*, "Baicalin induces ferroptosis in osteosarcomas through a novel Nrf2/xCT/GPX4 regulatory axis," *Phytomedicine* **116**, 154881 (2023).
10. Y Wen, Y. Wang, C. Zhao, *et al.*, "The Pharmacological Efficacy of Baicalin in Inflammatory Diseases," *Int. J. Mol. Sci.* **24**(11), 9317 (2023).
11. J Yuan, S. U. Khan, J. Yan, *et al.*, "Baicalin enhances the efficacy of 5-Fluorouracil in gastric cancer by promoting ROS-mediated ferroptosis," *Biomed. Pharmacother.* **164**, 114986 (2023).
12. C Wang, Y. Yang, L. Sun, *et al.*, "Baicalin reverses radioresistance in nasopharyngeal carcinoma by downregulating autophagy," *Cancer Cell Int.* **20**(1), 35 (2020).
13. L Zhang, G. Yu, Q Yu, *et al.*, "Baicalin promotes random-pattern skin flap survival by inducing autophagy via AMPK-regulated TFEB nuclear transcription," *Phytother. Res.* **37**(9), 3926–3938 (2023).
14. Y Cheng, M. Yan, S. He, *et al.*, "Baicalin alleviates angiotensin II-induced cardiomyocyte apoptosis and autophagy and modulates the AMPK/mTOR pathway," *J. Cell. Mol. Med.* **28**(9), e18321 (2024).
15. Y Shi, S. Chen, R. B. Liu, *et al.*, "The new insights into autophagy in thyroid cancer progression," *J. Transl. Med.* **21**(1), 413 (2023).
16. Y Wang, Z. Cao, T Yu, *et al.*, "Enhancement of the superprism effect based on the strong dispersion effect of ultrahigh-order modes," *Opt. Lett.* **33**(11), 1276 (2008).
17. Y Zheng, Z. Cao, X Chen, *et al.*, "Conical reflection of light during free-space coupling into a symmetrical metal-cladding waveguide," *J. Opt. Soc. Am. A* **30**(9), 1901 (2013).
18. R. Horvath, H. C. Pedersen, and N. B. Larsen, "Demonstration of reverse symmetry waveguide sensing in aqueous solutions," *Appl. Phys. Lett.* **81**(12), 2166–2168 (2002).
19. T Li, J. Fan, B Wang, *et al.*, "TIMER: a web server for comprehensive analysis of tumor-infiltrating immune cells," *Cancer Res.* **77**(21), e108–e110 (2017).
20. T Li, J. Fu, Z Zeng, *et al.*, "TIMER2.0 for analysis of tumor-infiltrating immune cells," *Nucleic. Acids Res.* **48**(W1), W509–W514 (2020).
21. F Bruno, P. Abondio, A Montesanto, *et al.*, "The Nerve Growth Factor Receptor (NGFR/p75 NTR): A Major Player in Alzheimer's Disease," *Int. J. Mol. Sci.* **24**(4), 3200 (2023).
22. T Siddiqui, M. I. Cosacak, S Popova, *et al.*, "Nerve growth factor receptor (Ngfr) induces neurogenic plasticity by suppressing reactive astroglial Lcn2/Slc22a17 signaling in Alzheimer's disease," *npj Regener. Med.* **8**(1), 33 (2023).
23. S Garcia-Silva, L. Benito-Martin, S Nogués, *et al.*, "Melanoma-derived small extracellular vesicles induce lymphangiogenesis and metastasis through an NGFR-dependent mechanism," *Nat. Cancer* **2**(12), 1387–1405 (2021).
24. J Lehmann, N. Caduff, E Krzywińska, *et al.*, "Escape from NK cell tumor surveillance by NGFR-induced lipid remodeling in melanoma," *Sci. Adv.* **9**(2), eadc8825 (2023).
25. BR Pflug and M Onoda, "Reduced expression of the low affinity nerve growth factor receptor in benign and malignant human prostate tissue and loss of expression in four human metastatic prostate tumor cell line," *Cancer Res.* **52**(19), 5403–5406 (1992).
26. J Boshuizen, O. Vredevoogd, J Krijgsman, *et al.*, "Reversal of pre-existing NGFR-driven tumor and immune therapy resistance," *Nat. Commun.* **11**(1), 3946 (2020).
27. G Vitale, A Dicitore, and D. Pepe, "Synergistic activity of everolimus and 5-aza-2'-deoxycytidine in medullary thyroid carcinoma cell lines," *Mol. Oncol.* **11**(8), 1007–1022 (2017).
28. S Faulkner, Philip Jobling, and Christopher W Rowe, "Neurotrophin Receptors TrkA, p75NTR, and Sortilin Are Increased and Targetable in Thyroid Cancer," *Am. J. Pathol.* **188**(1), 229–241 (2018).
29. W Chai, F. Ye, L Zeng, *et al.*, "HMGB1-mediated autophagy regulates sodium/iodide symporter protein degradation in thyroid cancer cells," *J. Exp. Clin. Cancer Res.* **38**(1), 325 (2019).
30. K Liu, Q. Yu, H Li, *et al.*, "BIRC7 promotes epithelial-mesenchymal transition and metastasis in papillary thyroid carcinoma through restraining autophagy," *Am. J. Cancer Res.* **10**(1), 78–94 (2020).